Journal of Manufacturing Processes 39 (2019) 346–355

Contents lists available at ScienceDirect

Journal of Manufacturing Processes

journal homepage: www.elsevier.com/locate/manpro

A study on the production of thin-walled Ti6Al4V parts by selective laser melting

G. Miranda[a,*], S. Faria[b], F. Bartolomeu[a], E. Pinto[c], N. Alves[c], N. Peixinho[d], M. Gasik[e], F.S. Silva[a]

[a] Center for Micro-Electro Mechanical Systems (CMEMS-UMinho), University of Minho, Campus de Azurém, 4800-058, Guimarães, Portugal
[b] CMAT - Centre of Mathematics, Department Mathematics and Applications, University of Minho, Campus de Azurém, 4800-058, Guimarães, Portugal
[c] Centre for Rapid and Sustainable Product Development (CDRSP), Polytechnic Institute of Leiria, Rua General Norton de Matos, Apartado 4133, 2411-901, Leiria, Portugal
[d] Mechanical Engineering and Resource Sustainability Centre (MEtRICs-UMinho), University of Minho, Campus de Azurém, 4800-058, Guimarães, Portugal
[e] Department of Materials Science and Engineering, School of Chemical Technology, Aalto University Foundation, 00076, Aalto, Espoo, Finland

ARTICLE INFO

Keywords:
Ti6Al4V
Selective laser melting
Thin-walled parts

ABSTRACT

Selective Laser Melting (SLM) is an extremely versatile technology especially suited for the manufacturing of thin-walled parts. Micro-sized parts are highly influenced and dependent on the SLM processing parameters; thus being indispensable to assess the influence of processing parameters on SLM fabrication, as isolated parameters but also their interactions. In this study, the influence of SLM laser power and scanning speed on Ti6Al4V micro-pillars and micro-plates thickness was assessed by applying response surface methodology (RSM). These analyses resulted in four models that exhibit complex correlations of SLM process parameters, with non-linear equations, having coefficients of determination that assess the quality of the models. These developed models are accurate tools that can be used to optimize the micro manufacture of Ti6Al4V thin-walled parts by SLM.

1. Introduction

Selective laser melting (SLM) is an additive manufacturing process that builds parts layer-by-layer, allowing the production of complex structures, like free-form enclosed structures and thin-walled channels, with high material savings, once it is able to reuse the non-melted powder (95–98% recyclability for metal powders) [1]. By SLM, a direct production from 3D CAD model is performed. Layer upon layer of powder (corresponding to slices of the model) are deposited and then a laser beam scans over each layer of powder using a predefined path and using selected SLM parameters in order to melt and bond the melted layer to the previous one [2,3].

Ti6Al4V is a titanium alloy abundantly used in biomedical applications mainly due to its high corrosion resistance, chemical stability, biocompatibility and mechanical properties [4]. Ti6Al4V parts produced by SLM are highly dependent on SLM processing parameters, especially laser power, scan speed, scan spacing, powder layer thickness and laser spot size [5]. Several studies regarding Ti6Al4V produced by SLM are found in literature, whether verifying how the SLM parameters influence density [5] or assessing their mechanical properties [6–8]. Furthermore, SLM accuracy is a present challenge to the fabrication of Ti6Al4V parts and especially thin-walled parts, once noteworthy dimensional deviations are systematically detected between the CAD model and the produced parts [9–11]. In fact, the use of SLM as a mainstream manufacturing method for metals in general and Ti6Al4V in particular, demand a great understanding of the process, in order to increase quality, repeatability, and overcome the scarcity of standards [12]. In this sense the use of models that can predict the influence of SLM parameters on a given property is an efficient approach for an optimized SLM production. Furthermore, models are powerful tools for the design of optimized parts, avoiding over extensive experimental testing but instead using available knowledge for a given material. In fact some models regarding parts produced by SLM have been developed [12–14], but for thin structures literature is scarce.

Response surface methodology (RSM) is a collection of statistical and mathematical techniques useful for the modeling and analysis of problems in which a response of interest is influenced by several variables and the objective is to optimize this response [13]. Regarding thin-walled parts, regression models can be useful for correlating input data like SLM processing parameters and output data like thickness.

This work intends to investigate SLM technology capability to fabricate Ti6Al4V thin-walled parts, namely micro-pillars and micro-plates and to assess the influence of laser power and scan speed on these micro-sized parts dimensions and also on their roughness. In this sense,

* Corresponding author.
E-mail address: gmiranda@dem.uminho.pt (G. Miranda).

https://doi.org/10.1016/j.jmapro.2018.12.036
Received 21 September 2017; Received in revised form 18 December 2018; Accepted 27 December 2018
Available online 12 March 2019

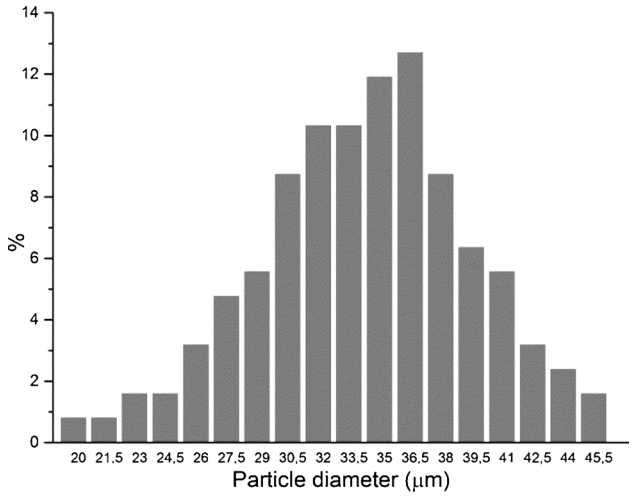

Fig. 1. Size distribution of the Ti6Al4V powder.

analysis of variance (ANOVA) for quadratic regression models were obtained, for micro-pillars and micro-plates, considering their melt zone thickness or their total thickness. These analyses assessed the effect of significant main factors and their interactions, allowing determining the optimal working conditions for achieving parts with a given thickness and the minimum thickness achievable. These models can be used to optimize thin-walled parts fabrication.

2. Experimental procedure

2.1. Material and processing details

Ti6Al4V powdered alloy purchased from SLM Solutions GmbH, Germany was used to produce the micro-pillars and micro-plates. The Ti6Al4V spherical powder size distribution, according to the manufacturer, is presented in Fig. 1.

Ti6Al4V micro-pillars and micro-plates were produced on a SLM equipment from SLM Solutions (model 125 H L). This equipment, equipped with a Yb-Faser-Laser having a spot of 87 μm, provides an inert gas flow during the production of the parts. More details on this equipment are found elsewhere [13].

For the production of these specimens, a powder layer thickness of 30 μm was used, while scan spacing was maintained constant. The platform temperature was maintained constant at 200 °C. The laser path used for these parts production is presented in Fig. 2.

The plan of experiments for the production of the micro-pillars and micro-plates is shown on Table 1, with processing parameters variation selected in order to assess the influence of laser power and scan speed on the obtained specimen's thickness and roughness.

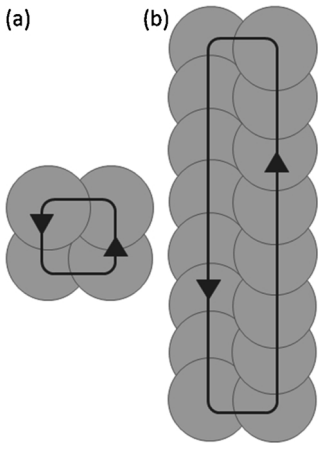

Fig. 2. Laser path used for the fabrication of the (a) micro-pillars and (b) micro-plates.

Table 1
Plan of experiments for Ti6Al4V micro-pillars and micro-plates fabrication.

Experiment	A Power [W]	B Scan speed [mm/s]
1	50	300
2	50	400
3	60	300
4	60	400
5	60	500
6	60	600
7	60	700
8	70	400
9	70	550
10	80	300
11	80	400
12	80	500
13	80	600
14	80	700
15	80	800
16	90	600
17	90	700
18	90	1250
19	100	300
20	100	400
21	100	500
22	100	600
23	100	700
24	100	1250

The micro-pillars and micro-plates were produced with an average height of 5 mm (not including the supports) and regarding the micro-plates with a width of 5 mm. Fig. 3 shows the micro-pillars (Fig. 3(a)) and the micro-plates (Fig. 3(b)) after fabrication, still in the production platforms.

This study investigates SLM technology capability to fabricate Ti6Al4V micro-pillars and micro-plates with thicknesses between 100 and 300 μm, assessing the optimum parameters combination for the production of any given thickness and especially the minimum thickness when using a laser beam with a spot diameter of 87 μm, typically found in commercial equipment's.

2.2. Roughness and thickness analysis

After fabrication, the micro-plates were cut from the production platform and their roughness was measured using a surface profilometer (Surftest SJ 201, Mitutoyo). Roughness measurements were performed in the two directions schematically depicted in Fig. 4 (and named horizontal and vertical). The roughness tests were performed by following ISO 4287:1997, with an evaluation length of 3 mm at 0.1 mm/s and three profiles were performed in different areas for each direction. Besides Ra and Rz calculation, the profilometry was also recorded.

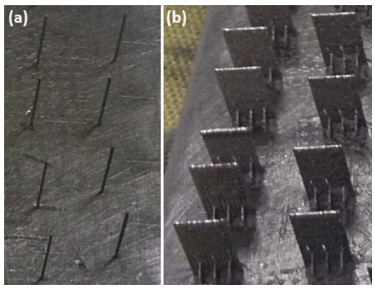

Fig. 3. Ti6Al4V (a) micro-pillars and (b) micro-plates after SLM fabrication.

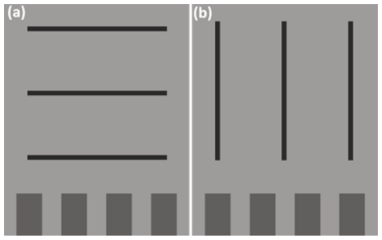

Fig. 4. Roughness measurement directions: (a) horizontal and (b) vertical.

Micro-plates and micro-pillars were analyzed by Scanning Electron Microscopy (SEM) in order to perform thickness measurements. For each experiment (for micro-pillars and micro-plates) thickness results were obtained as an average of four measurements in the case of micro-pillars and eight for micro-plates. The SEM images acquired in the top face of the micro-pillars and micro-plates allow the analysis on these specimens of the laser spot path, the laser spot diameter and the scan spacing. Two types of thickness measurements were performed on the micro-pillars and on the micro-plates: the melt zone thickness (white arrows marked in Fig. 5) and their total thickness (contemplating the black and white arrows in Fig. 5).

2.3. Statistical analysis

Multiple regression analysis was applied to the experimental data obtained as described above, in order to obtain the mathematical models for the responses (melt zone and total thickness) as a function of the selected variables (laser power and scan speed).

The most common model which is used to describe the relation between independent variables and the response variable is the quadratic regression model which can be expressed by Eq. (1):

$$Y = b_0 + \sum_{i=1}^{k} b_i X_i + \sum_{i=1}^{k} b_{ii} X_i^2 + \sum_{i=1}^{k-1} \sum_{j>i}^{k} b_{ij} X_i X_j + \varepsilon \quad (1)$$

where Y denotes the response (dependent) variables, k the number of independent variables, b_0 the constant, ε the residual (error) term, b_i the linear coefficient, b_{ii} the quadratic coefficient, b_{ij} the interaction coefficient and X_i, X_j dimensionless coded independent variables.

The quadratic regression model is flexible, because it can take a variety of functional forms and approximates the response surface locally. Therefore, this model is usually a good estimation of the true response surface.

In order to find the significant variables affecting the response variable, Analysis of Variance (ANOVA) was performed. The coefficients of determination (R^2) were used to assess the quality of the models and a test for lack-of-fit was implemented in order to assess if there are contributions in the regressor–response relationship not accounted by the models. The adequacy of the models was also investigated by the examination of residuals.

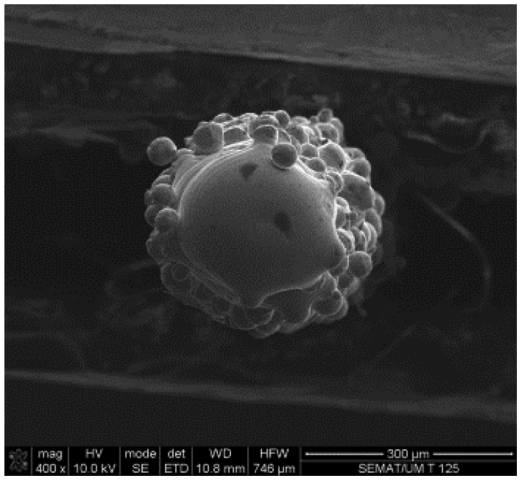

Fig. 6. Ti6Al4V micro-pillar from experiment 8.

3. Results and discussion

SEM images of the produced micro-pillars and micro-plates (with two examples being shown on Figs. 6 and 7) show no substantial constructive defects and porosity, assessing the effectiveness of the SLM process for the fabrication of these parts.

Parts obtained by SLM are distinguishable by a rough surface due the fact that around a melted volume takes place a partial melting of particles from the vicinity powder, conferring to these parts a typical outer surface. Fig. 8 shows some of the lateral surfaces of micro-plates of experiment number 1, 7 and 10, made with different processing parameters (see Table 1). The roughness of these surfaces was measured in the horizontal direction (parallel to the melted layers of powder) and vertical direction (perpendicular to the melted layers of powder). The average results for Ra are presented in Table 2, for micro-plates of experiment number 1, 7 and 10.

The roughness measurements presented in Table 2 show that by using different processing parameters no clear tendency is found, since this roughness is mostly dependent on the diameter of the Ti6Al4V particles used. The differences here observed can be explained based on the powder size distribution shown in Fig. 1. Comparing this roughness with the micro-plates thickness (presented on the next section), it appears that this rough surface (beyond the melt zone) constitutes, on average, approximately 30% of the total thickness.

3.1. Statistical analysis of the thickness results

Regression models were developed using the input (processing parameters) shown in Table 1 and the output data (thickness results) depicted in Fig. 9.

ANOVA for quadratic regression models were obtained for the micro-pillars and micro-plates melt zone thickness and their total thickness. These analyses estimated the effect of significant variables laser power (A) and scan speed (B) and their interaction. The developed

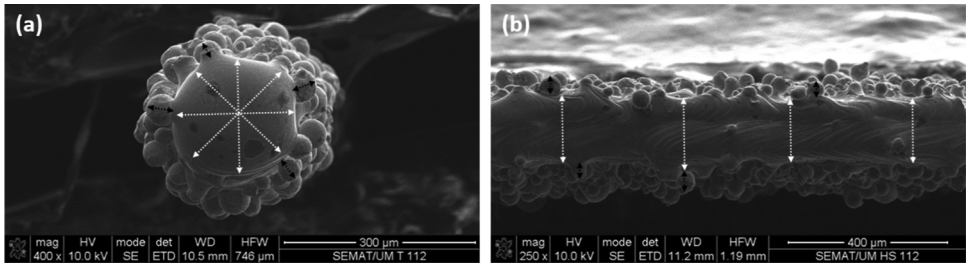

Fig. 5. Melt zone and total thickness measurements on Ti6Al4V (a) micro-pillars and (b) micro-plates.

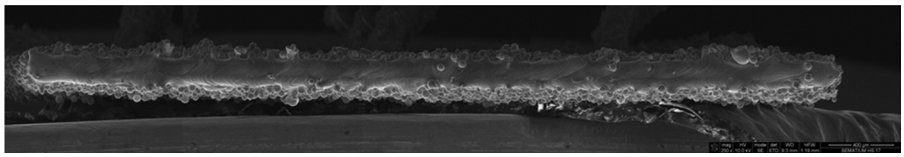

Fig. 7. Ti6Al4V micro-plate from experiment 1.

models allow determining the optimal working conditions for achieving parts with a given thickness and the minimum thickness achievable when using a laser spot of 87 μm.

3.1.1. Micro-plates

Regarding the micro-plates, two quadratic models were developed: one for the melt zone thickness (Eq. (2)) and other for their total thickness (Eq. (3)).

$$Melt\ thickness = 153.5402 + 36.1969A - 7.7619B + 4.2750AB + 10.7766A^2 \quad (2)$$

$$Thickness = 202.6007 + 10.5780A - 6.4063B - 4.2314AB + 7.9886A^2 + 0.\ 8277B^2 \quad (3)$$

The results of the ANOVA analysis for the melt thickness and the total thickness of the micro-plates are found on Tables 3 and 4

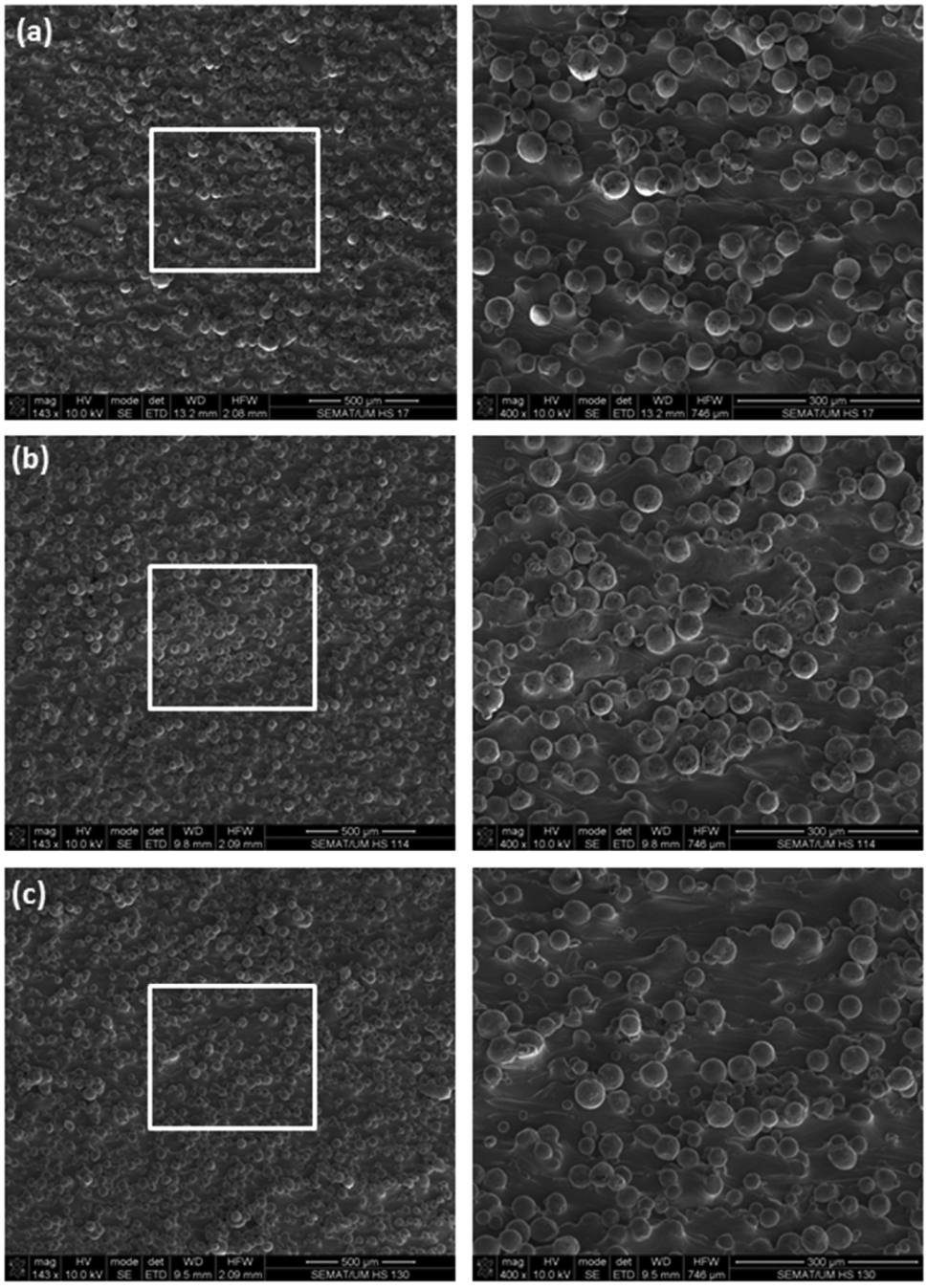

Fig. 8. Lateral view of micro-plates of experiment number (a) 1, (b) 7 and (c) 10.

Table 2
Roughness (Ra) acquired for micro-plates (in the horizontal and vertical direction).

Micro-plate of experiment	Ra [μm]	
	Horizontal	Vertical
1	14.564 ± 1.289	17.826 ± 2.143
7	13.127 ± 0.767	13.211 ± 0.732
10	14.805 ± 1.232	16.587 ± 1.052

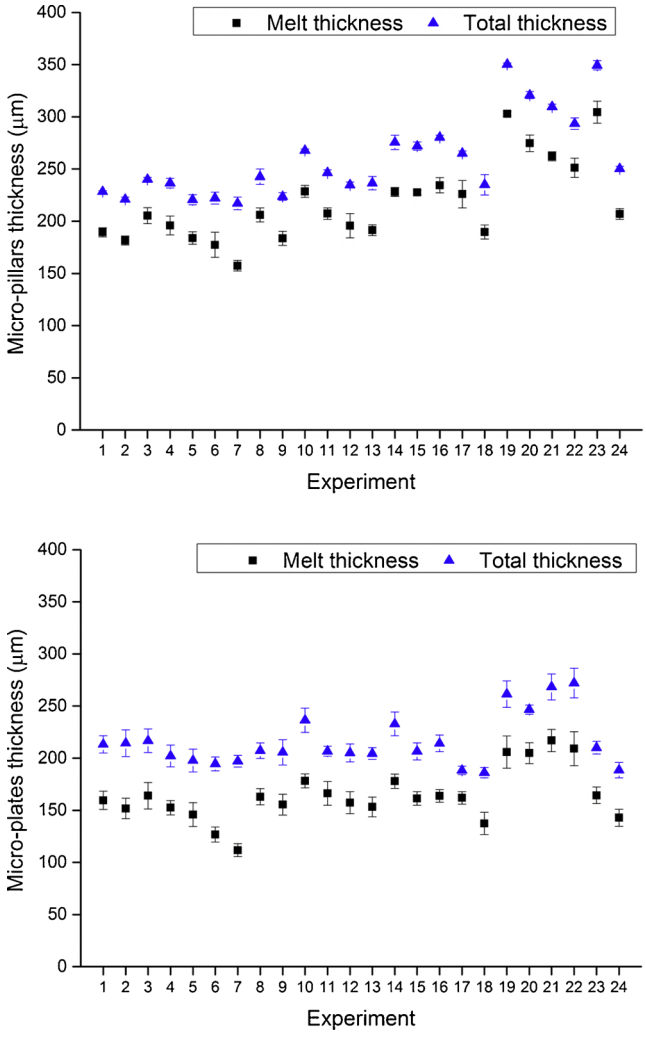

Fig. 9. Ti6Al4V micro-pillars and micro-plates average thickness (melt zone and total).

respectively.

The probability values (< 0.05) found for these two models show that A, B, AB and A^2 terms are the significant model terms for the melt thickness model, while A, B, AB, A^2 and B^2 are the significant model terms for the thickness model.

The F values obtained for these models were 50.53 (melt thickness model) and 25.87 (thickness model), both indicating that the models are significant. On the other hand, lack-of-fit F values of 0.5105 (melt thickness model) and 1.5346 (thickness) indicate that lack of fit is non-significant, as desirable.

As seen in Tables 3 and 4, the values found for R^2, adjusted R^2 and predicted R^2 are all in good agreement, confirming that the predicted models for the micro-plates melt thickness and for the total thickness can be employed. Furthermore, the adequate precision value for the

Table 3
ANOVA and regression analysis summary for the melt thickness of micro-plates.

Model terms	Sum of Squares	Degree of freedom	Mean Square	F value	P-value
Model	13663.31	4	3415.828	50.53	< 0.001
A	9171.2	1	9171.2	135.6982	< 0.001
B	4054.6	1	4054.6	59.992	< 0.001
AB	579.9	1	579.9	8.5796	0.008
A^2	893.5	1	893.5	13.220	0.002
Residuals	1486.9	22	67.6		
Lack of fit	776.8	15	51.8	0.5105	0.870
Pure error	710.1	7	101.4		
Cor. total	15150.21	26			
Press	2044.575				

R^2: 0.9018.
Adjusted R^2: 0.8840.
Predicted R^2: 0.8650.
Adequate precision: 26.81.

Table 4
ANOVA and regression analysis summary for the thickness of micro-plates.

Model terms	Sum of Squares	Degree of freedom	Mean Square	F value	P-value
Model	6320.041	5	1264.008	25.87	< 0.001
A	759.26	1	759.26	15.5394	< 0.001
B	2632.92	1	2635.92	53.8868	< 0.001
AB	572.6	1	572.6	11.7194	0.003
A^2	432.7	1	432.7	8.8554	0.007
B^2	665.9	1	665.9	13.6283	0.002
Residuals	1074.9	22	48.86		
Lack of fit	824.3	15	54.95	1.5346	0.291747
Pure error	250.7	7	35.81		
Cor. total	7394.941	27			
Press	1529.002				

R^2: 0.8547.
Adjusted R^2: 0.8216.
Predicted R^2: 0.7933.
Adequate precision: 22.71.

melt thickness model equation was 26.81, while for the thickness model was of 22.71. Both these values allow concluding that the signal is adequate, assuring a reasonable performance according to the prediction, for both models.

Figs. 10 and 11 depict the normal probability plots of the residuals and the plots of the residuals versus the predicted response for the two obtained models for the micro-plates. The normal probability plots of Fig. 10 and 11 confirm that the residuals mostly fall on a straight line, inferring that the errors are distributed normally. On the other hand, the plots of the residuals versus the predicted response haven't revealed noticeable patterns, thus indicating that the two models are adequate.

3.1.2. Micro-pillars

Concerning the micro-pillars, again two models were developed: melt zone thickness and their total thickness. Below are the quadratic models (Eqs. (4) and (5)) that were shown to fit the data appropriately:

$$Melt\ thickness = 192.111 + 38.484A - 9.955B - 3.649AB + 16.966A^2 + 1.116B^2 \quad (4)$$

$$Thickness = 235.222 + 36.707A - 7.98019B - 6.240AB + 20.138A^2 + 1.1783B^2 \quad (5)$$

The results of the ANOVA analysis for the melt thickness and the total thickness of the micro-pillars are found on Tables 5 and 6 respectively.

The probability values (< 0.05) found for these two models show that A, B, AB, A^2 and B^2 terms are the significant model terms for the melt thickness model, and A, B, AB and A^2 and B^2 are the significant

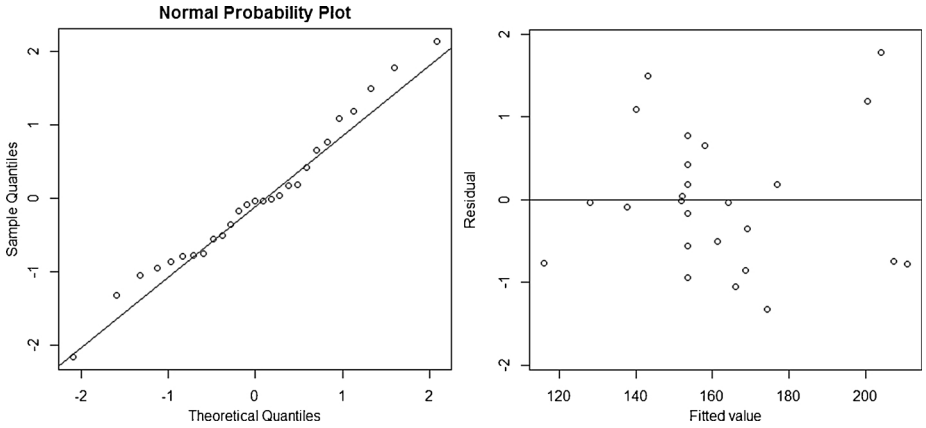

Fig. 10. Normal probability plot of residuals and plot of residuals vs. fitted value for melt thickness of micro-plates data.

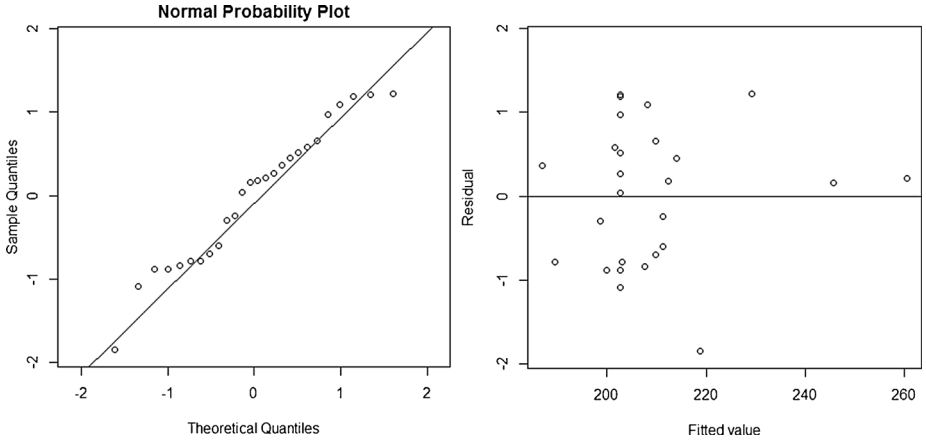

Fig. 11. Normal probability plot of residuals and plot of residuals vs. fitted value for total thickness of micro-plates data.

Table 5
ANOVA and regression analysis summary for the melt thickness of micro-pillars.

Model terms	Sum of Squares	Degree of freedom	Mean Square	F value	P-value
Model	25984.8	5	5196.96	120.3	< 0.001
A	9535.9	1	9535.9	220.9914	< 0.001
B	5479.4	1	5479.4	126.9839	< 0.001
AB	362.4	1	362.4	8.3989	< 0.001
A^2	1989.6	1	1989.6	46.108	< 0.001
B^2	950.6	1	950.6	22.029	< 0.001
Residuals	690.4	16	43.2		
Lack of fit	581.5	13	44.7	1.2325	0.490
Pure error	108.9	3	36.3		
Cor. total	26675.2	21			

R^2: 0.9741.
Adjusted R^2: 0.9660.
Predicted R^2: 0.9516.
Adequate precision: 38.85.

Table 6
ANOVA and regression analysis summary for the thickness of micro-pillars.

Model terms	Sum of Squares	Degree of freedom	Mean Square	F value	P-value
Model	26608.5	5	5321.7	131.4	< 0.001
A	8675.2	1	8675.2	214.290	< 0.001
B	3521.0	1	35.21.0	86.9749	< 0.001
AB	1059.8	1	1059.8	26.1794	< 0.001
A^2	2803.1	1	2803.1	69.2410	< 0.001
B^2	981.2	1	981.2	24.2378	< 0.001
Residuals	647.7	16	40.5		
Lack of fit	482.3	13	37.1	0.6729	0.736
Pure error	165.4	3	55.1		
Cor. total	27256.2	21			

R^2: 0.9762.
Adjusted R^2: 0.9688.
Predicted R^2: 0.9612.
Adequate precision: 38.28.

model terms for the thickness model.

The F values obtained for these models were 120.3 (melt thickness model) and 131.4 (thickness model), both indicating that the models are significant. On the other hand, lack-of-fit F values of 1.2325 (melt thickness model) and 0.6729 (thickness) indicate that lack of fit is non-significant, as desirable.

As seen in Tables 5 and 6, the values found for R^2, adjusted R^2 and predicted R^2 are all in good agreement, confirming that the predicted models for the micro-pillars melt thickness and for the total thickness can be employed. Furthermore, the adequate precision value for the melt thickness model equation was 38.85, while for the thickness model was of 38.28. Both these values allow concluding that the signal is adequate, assuring a reasonable performance according to the prediction, for both models.

Figs. 12 and 13 depict the normal probability plots of the residuals and the plots of the residuals versus the predicted response for the two obtained models for the micro-pillars. The normal probability plots of Figs. 12 and 13 confirm that the residuals mostly fall on a straight line, inferring that the errors are distributed normally. On the other hand, the plots of the residuals versus the predicted response haven't revealed noticeable patterns, thus indicating that the two models are adequate.

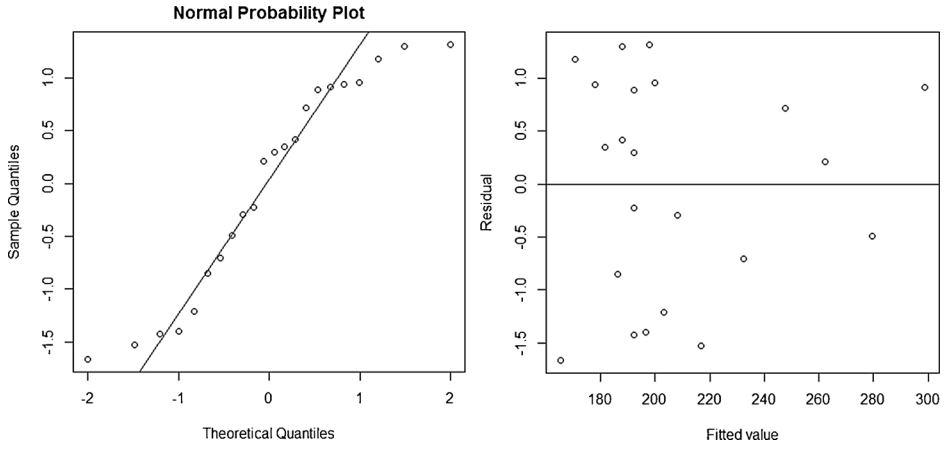

Fig. 12. Normal probability plot of residuals and plot of residuals vs. fitted value for melt thickness of micro-pillars data.

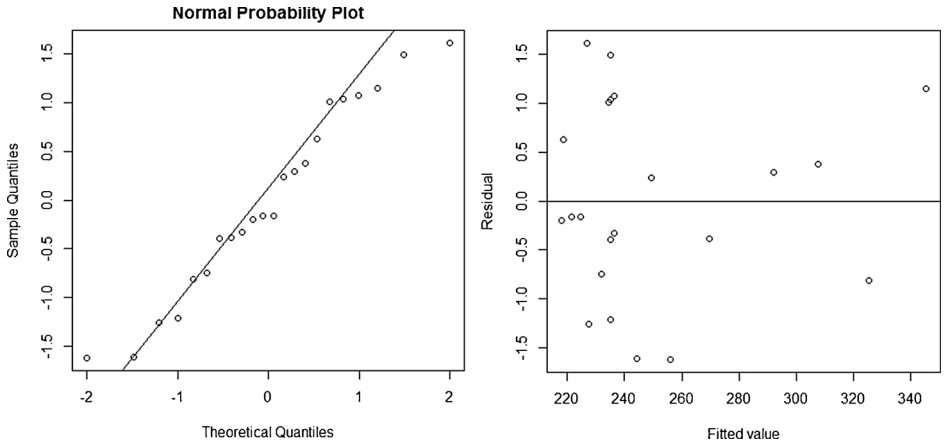

Fig. 13. Normal probability plot of residuals and plot of residuals vs. fitted value for total thickness of micro-pillars data.

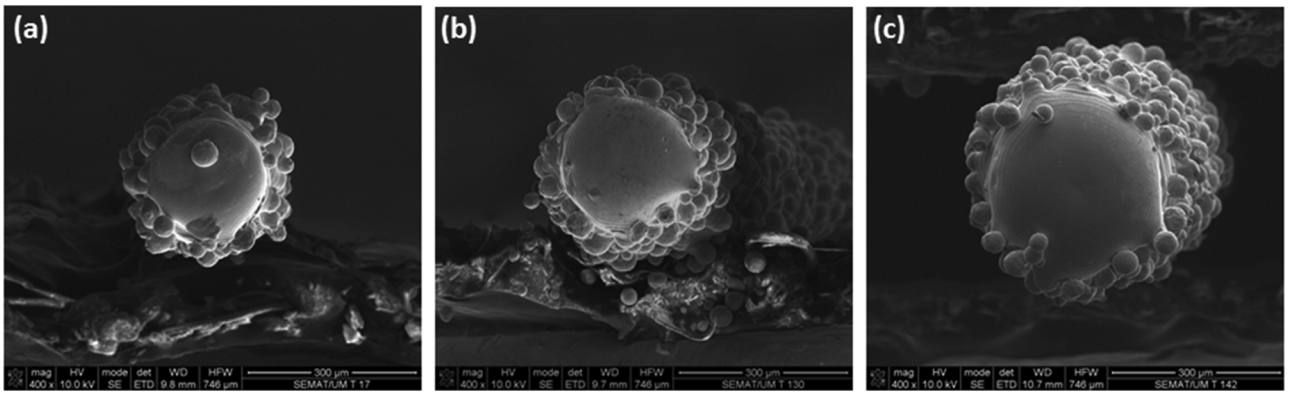

Fig. 14. Micro-pillars built on experiment number (a) 1 (50 W), (b) 10 (80 W) and (c) 19 (100 W).

3.2. Models coefficients and parameters influence

All the developed models, for micro-pillars and micro-plates, show that laser power and scan speed have a significant effect on the thickness of the produced specimens, as regarding the melt zone thickness and the total thickness. The coefficients of laser power (A) and scan speed (B) parameters on the four developed models prove these parameters single influence.

Regarding laser power, all models showed that by increasing power, for the tested power intervals, higher thicknesses (melt zone and total) are obtained, as proven by the positive and expressive values obtained for the coefficients of laser power (A). Higher energy density, promoted by increasing laser power, promotes a larger melt pool, thus leading to thicker parts. In fact, when observing Fig. 14(a), (b) and (c), corresponding to micro-pillars produced with the same scan speed (300 mm/s) but differing in the laser power that was used (50, 80 and 100 W) it can be verified that a gradual increase on the melt zone occurs when increasing the laser power.

Regarding micro-plates a similar trend can be observed when analyzing Fig. 15, where micro-plates produced using the same scan speed (400 mm/s) and varying laser power (50, 80 and 100 W) are presented.

Concerning scan speed, an opposite influence is observed, as evidenced by the negative coefficients found for scan speed (B) in all the developed models. Thus, when increasing speed, lower thicknesses

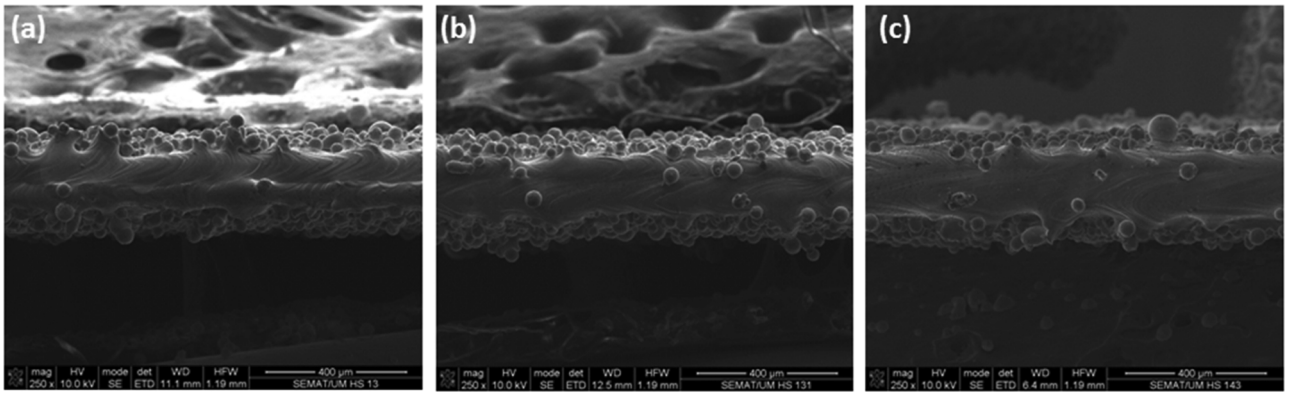

Fig. 15. Micro-plates built on experiment number (a) 2 (50 W), (b) 11 (80 W) and (c) 20 (100 W).

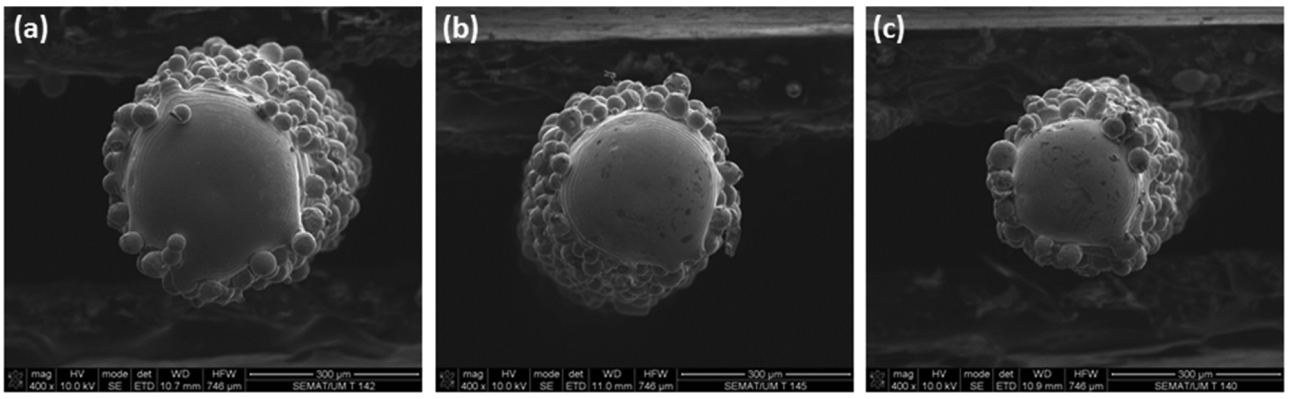

Fig. 16. Micro-pillars built on experiment number (a) 19 (300 mm/s), (b) 22 (600 mm/s) and (c) 24 (1250 mm/s).

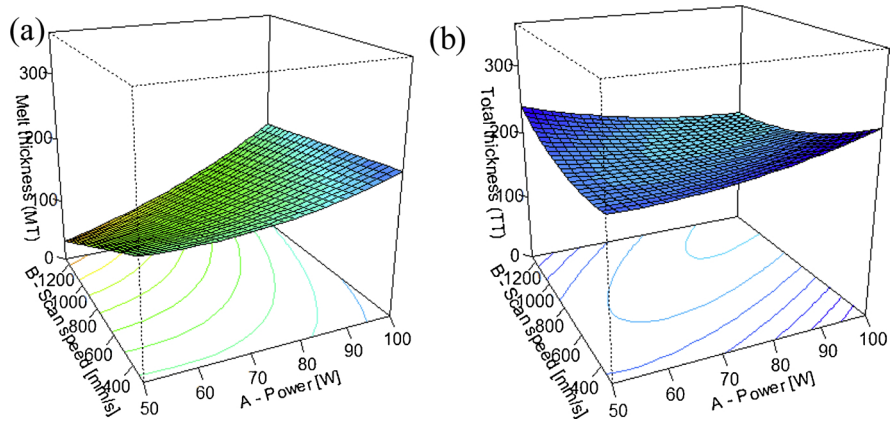

Fig. 17. 3D response surface plots for the micro-plates (a) melt thickness and (b) thickness models.

(melt zone and total) are obtained. Again, energy density can explain this trend, once a lower energy density is delivered per second in a designated area, when the laser scan speed is increased. As an example, Fig. 16(a)–(c) shows micro-pillars produced with the same laser power (100 W) but differing in the scan speed that was used (300, 600 and 1250 mm/s), that prove the abovementioned scan speed influence on the thickness of these specimens, with lower speed generating parts with more melted material.

A comment on the laser power quadratic term (A^2), found significant in all of the four models that were developed must be done, once it was found that this term coefficients were expressively high and with positive values, thus showing a higher influence of laser power on these parts thickness, when comparing with scan speed (B).

All the four models obtained showed that there are interactions between the two independent variables, laser power (A) and scan speed (B) (see Tables 3–6). Figs. 17 and 18 show the 3D response surface plots for the micro-plates and micro-pillars melt thickness and thickness models.

From Figs. 17 and 18 it is possible to conclude that for both the melt and total thicknesses models there is a tendency for higher thickness with increasing power, for any scan speed from the selected range. These results are due to the higher energy density, promoted by

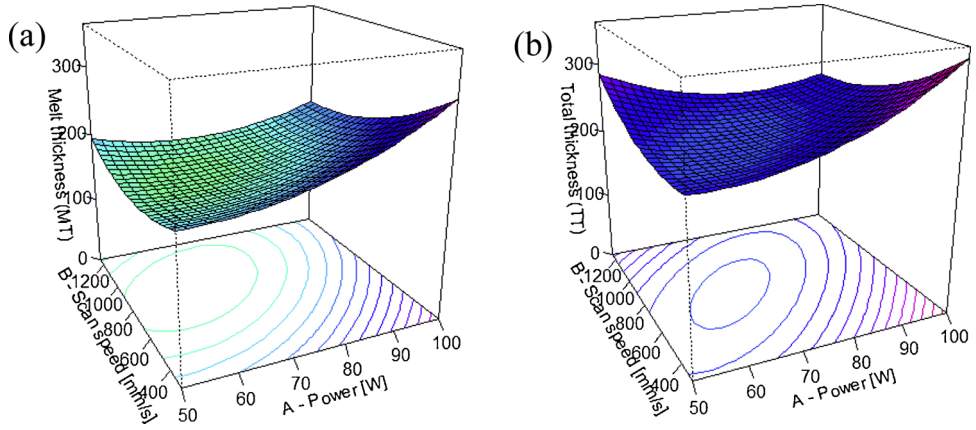

Fig. 18. 3D response surface plots for the micro-pillars (a) melt thickness model and (b) thickness model.

increasing laser power, that promote a larger melt pool, thus leading to thicker parts. Regarding the scan speed influence, a tendency for obtaining higher thickness is found when using lower scan speed, especially when these are applied together with high laser power.

From the previous models it can be seen that, contrarily to what occurs on macro-sized parts, for micro-sized parts, final dimensions are extremely dependent on process variables, namely on power and scan speed. Thus, for micro-sized parts, particular attention must be paid to SLM processing parameters.

4. Conclusions

The main conclusions that can be drawn from this work are:

- Models on the influence of SLM processing parameters laser power and scan speed (independent variables) on the thickness (dependent variable) of micro-pillars and micro-plates made of Ti6Al4V alloy were developed;
- All the obtained models exhibit complex correlations of SLM process parameters, with non-linear equations;
- The developed models are accurate tools that can be used to optimize the micro manufacture of Ti6Al4V thin-walled parts by SLM.

Acknowledgements

This work is supported by FCT - Fundação para a Ciência e a Tecnologia through the grant SFRH/BPD/112111/2015 and the projects PTDC/EMS-TEC/5422/2014 and NORTE-01-0145-FEDER-000018-HAMaBICo. Additionally, this work is supported by FCT with the reference project UID/EEA/04436/2013, by FEDER funds through the COMPETE 2020 – Programa Operacional Competitividade e Internacionalização (POCI) with the reference project POCI-01-0145-FEDER-006941.

References

[1] Ford S, Despeisse M. Additive manufacturing and sustainability: an exploratory study of the advantages and challenges. J Clean Prod 2016;137:1573–87.
[2] Edwards P, Ramulu M. Fatigue performance evaluation of selective laser melted Ti-6Al-4V. Mater Sci Eng A 2014;598:327–37.
[3] Zhang H, Zhu H, Qi T, Hu Z, Zeng X. Selective laser melting of high strength Al–Cu–Mg alloys: processing, microstructure and mechanical properties. Mater Sci Eng A 2016;656:47–54.
[4] Strnad G, Chirila N. Corrosion rate of sand blasted and acid etched Ti6Al4V for dental implants. Procedia Technol 2015;19:909–15.
[5] Sun J, Yang Y, Wang D. Parametric optimization of selective laser melting for forming Ti6Al4V samples by Taguchi method. Opt Laser Technol 2013;49:118–24.
[6] Zhang S, Wei Q, Cheng L, Li S, Shi Y. Effects of scan line spacing on pore characteristics and mechanical properties of porous Ti6Al4V implants fabricated by selective laser melting. Mater Des 2014;63:185–93.
[7] Wauthle R, Vrancken B, Beynaerts B, Jorissen K, Schrooten J, Kruth J-P, et al. Effects of build orientation and heat treatment on the microstructure and mechanical properties of selective laser melted Ti6Al4V lattice structures. Addit Manuf 2015;5:77–84.
[8] Simonelli M, Tse YY, Tuck C. Effect of the build orientation on the mechanical properties and fracture modes of SLM Ti6Al4V. Mater Sci Eng A 2014;616:1–11.
[9] Arabnejad S, Johnston RB, Ann J, Singh B, Tanzer M, Pasini D. High-strength porous biomaterials for bone replacement: a strategy to assess the interplay between cell morphology, mechanical properties, bone ingrowth and manufacturing constraints. Acta Biomater 2016;30:345–56.
[10] Bagheri ZS, Melancon D, Liu L, Johnston RB, Pasini D. Compensation strategy to reduce geometry and mechanics mismatches in porous biomaterials built with selective laser melting. J Mech Behav Biomed Mater 2017;70:17–27.
[11] Bartolomeu F, Sampaio M, Carvalho O, Pinto E, Alves N, Gomes JR, et al. Tribological behavior of Ti6Al4V cellular structures produced by Selective Laser Melting. J Mech Behav Biomed Mater 2017;69:128–34.
[12] Tapia G, Elwany AH, Sang H. Prediction of porosity in metal-based additive manufacturing using spatial Gaussian process models. Addit Manuf 2016;12:282–90.
[13] Miranda G, Faria S, Bartolomeu F, Pinto E, Madeira S, Mateus A, et al. Predictive models for physical and mechanical properties of 316L stainless steel produced by selective laser melting. Mater Sci Eng A 2016;657:43–56.
[14] Bartolomeu F, Faria S, Carvalho O, Pinto E, Alves N, Silva FS, et al. Predictive models for physical and mechanical properties of Ti6Al4V produced by selective laser melting. Mater Sci Eng A 2016;663:181–92.

Georgina Miranda is the Principal Investigator of FCT SR& TD Project "Development of smart designed adaptive prosthesis for Orthopaedic Applications (PTDC/EMS-TEC/5422/2014)", FCT post-doctoral fellow on the "Development of Multi-Functional Structures by Multi-Material Selective Laser Melting/Sintering" both at CMEMS – University of Minho (UM) and invited professor on the Dept. of Mechanical Engineering at UM. Georgina earned her PhD in Mechanical Engineering in 2015, working on the "Development of aluminum based composites by pressure-assisted sintering". Her main current interests include bioactive materials; biomedical alloys; laser sintering/melting; metallic cellular structures; FGMs and shape memory alloys. She currently has 27 papers published in ISI journals.

Susana Faria is an Auxiliary Professor at the Department of Mathematics and Applications of University of Minho (UM). She is author/co-author of more than 25 research papers in the fields of Statistics, Health and Life Science, Engineering and Social Sciences. She is the supervisor of several PhD and MSc students in the field of Statistics and her research interests include regression models and mathematical modelling.

Flávio Bartolomeu graduated in 2015, in Mechanical Engineering (Integrated Master) at the University of Minho with a master thesis on "Optimization of processing parameters on Laser Melting". Currently he is starting his PhD on CMEMS regarding "Ti-based cellular structures by SLS/SLM towards hip prosthesis design". On his PhD project an innovative additive manufacturing technology (multi-material selective laser sintering/melting) will be used to obtain Titanium-based cellular structured components. Functionally graded material (FGM) concept will also be used in his project, which is targeting to the development of improved hip prosthesis.

Elodie Pinto is a researcher member in the Centre for Rapid and Sustainable Product Development (CDRsp). She has a degree in Biomechanics and a Master degree in Engineering Design and Product Development, both from the Polytechnic Institute of Leiria. Her master thesis was entitled "Design and evaluation of multimaterial structures produced by stereo-thermal-lithography process". She has been developing research work on the Additive Fabrication Laboratory at CDRsp.

Nuno Alves is the Director of the Centre for Rapid and Sustainable Product Development (CDRsp) and Adjunct Professor on Computer Modelling and Simulation at Polytechnic Institute of Leiria. Nuno Alves co-edited four books, authored and co-authored more than 70 papers published in books, international journals, international conferences and 3 patents. He is involved in several research projects on the fields of Rapid Prototyping, Bio-Manufacturing and Reverse Engineering. Nuno Alves is Co-chair of the International Conference on Sustainable Intelligent Manufacturing (SIM) and Organizing Committee Member of the International Conference on Advanced Research in Virtual and Rapid Prototyping (VRAP).

Nuno Peixinho is currently Director of the PhD program in Mechanical Engineering and vice-director of the Integrated MSc program in Mechanical Engineering of the University of Minho. He holds a PhD degree in Mechanical Engineering from the University of Minho and his research field has been strongly tied with impact mechanics, dynamic material properties and cellular structures.

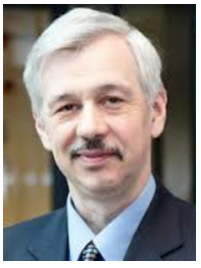

Michael Gasik is a worldwide expert on FGMs, member of the International Advisory Committee on Functional Gradated Materials (Japan) and honorary member of TechNet Alliance. Professor Gasik (Full Professor) is the head of the Materials Processing&Powder Metallurgy Research Group at Aalto University-Finland. With several decades of experience in FGMs, materials processing and biomaterials (inventor of novel in vitro biomaterials test BEST), he has over 250 publications and patents and carried out 8 EU projects, 2 IEA projects and 15 national projects. Professor Gasik works in new testing methods, elaboration of materials characterization and MODAO applications, with proper multiphysical modeling.

Filipe Silva is the head of the Micro Fabrication and Systems Integration Lab at CMEMS and Full Professor at the Department of Mechanical Engineering at University of Minho. With more than 15 years of experience in manufacturing processes by different technologies, including casting, powder metallurgy and laser sintering/melting, he has over 80 papers in ISI journals, 5 patents, 4 international awards for outstanding research & applied engineering and coordinated 16 research projects.